Rational Positioning of Metal Ions to Stabilize Open Tin Sites in Beta Zeolite for Catalytic Conversion of Sugars

*Pengyao Sun[+], Chong Liu[+], Haiyong Wang, Yuhe Liao, Xuning Li, Qiying Liu, Bert F. Sels, and Chenguang Wang**

Abstract: Via hydrothermal synthesis of Sn-Al gels, mild dealumination and ion exchange, a bimetallic Sn-Ni-Beta catalyst was prepared which can convert glucose to methyl lactate (MLA) and methyl vinyl glycolate (MVG) in methanol at yields of 71.2 % and 10.2 %, respectively. Results from solid-state magic-angle spinning nuclear magnetic resonance, X-ray photoelectron spectroscopy, transmission electron microscopy, spectroscopic analysis, probe-temperature-programmed desorption, and density functional theory calculations conclusively reveal that the openness of the Sn sites, such as by the formation of [$(SiO)_3$–Sn–OH] entities, is governed by an adjacent metal cation such as Ni^{2+}, Co^{2+}, and Mn^{2+}. This relies on the low structure-defective pore channel, provided by the current synthesis scheme, and the specific silica hydroxyl anchor point is associated with the incorporation of Sn for additional and precise metal ion localization. The presence of metal cations significantly improved the catalytic performance of Sn-Ni-Beta for glucose isomerization and conversion to MLA of sugar compared with Sn-Beta.

Introduction

Lewis acid sites are among the most important active centers on the surface of solid catalysts.[1] Isolated Sn sites in silicate BEA* zeolites as active Lewis acid centers[2] are particularly effective for the carbohydrates conversion, such as retro-aldol condensation[3,4] and sugar isomerization.[5] It has proved that in these reactions, the open form [$(SiO)_3$–Sn–OH] has a higher Lewis acidity and spatial flexibility than the closed form [$(SiO)_3$–Sn–OSi], resulting in higher reactivity.[4,6,7]

Static and dynamic examination of open and closed Sn sites is essential for the development of highly active and robust Sn-Beta catalysts as well as their application for industrial implementation.[8] The post-synthesis method is attractive by which the insertion of Sn into silica hydroxyl nests can lead to more open Sn sites than conventional hydrothermal synthesis method.[9,10] However, more silica hydroxyl groups will produce more dissociated H^+, which act as Brønsted acid and cause side reactions.[11–13] Moreover, the pores are hydrophilic due to the increased of silica hydroxyl groups, which stabilize the extended hydrogen-bonded network of water or alcohol during catalysis, and entropically destabilize the isomerized transition state.[14] Thus, it is quite challenging to precisely control open Sn sites number, preferably in a hydrophobic environment; however the factors that directly affect the proportion of open Sn sites were not explored thoroughly.

In fact, transition between open and closed Sn sites is very common in Sn-Beta. It depends on different synthesis schemes[15] and often influenced by the stability of the surrounding framework structure.[16] Bates et al.[17] showed that a defective open conformation can be formed when the Sn atom is present at the stacking fault of zeolite Beta, which has a similar coordination form to the open Sn site [$(SiO)_3$–Sn–OH], but the proximal Si–OH groups are not allowed to condense into the tetrahedral closed conformation. On the other hand, metal ions such as Na^+, K^+, Zn^{2+}, and Mg^{2+} can be incorporated flexibly into the zeolite, attaching to the terminal silica hydroxyl groups or forming extra-framework cations. Such incorporation can affect the local connectivity and the stability of the framework Sn.[6,18] Indeed, the enhancement of Sn-Beta catalytic efficiency by metal ions was reported. Tolborg et al.[13] increased methyl

[*] P. Sun,[+] H. Wang, Y. Liao, Prof. Q. Liu, Prof. C. Wang
CAS Key Laboratory of Renewable Energy, Guangdong Provincial Key Laboratory of New and Renewable Energy Research and Development, Guangzhou Institute of Energy Conversion, Chinese Academy of Sciences
No.2, Nengyuan Road, Wushan, Tianhe District, Guangzhou 510640 (China)
E-mail: wangcg@ms.giec.ac.cn

Dr. C. Liu[+]
State Key Laboratory of Structural Chemistry, Fujian Institute of Research on the Structure of Matter, Chinese Academy of Sciences
155 Yangqiao Road West, Fuzhou, 350002 (China)

Prof. X. Li
State Key Laboratory of Catalysis, Dalian Institute of Chemical Physics, Chinese Academy of Sciences
457 Zhongshan Road, Dalian 116023 (China)

Prof. B. F. Sels
Centre for Sustainable Catalysis and Engineering (CSCE), Leuven Chem&Tech, KU Leuven
Celestijnenlaan 200F, 3001 Heverlee (Belgium)

[+] These authors contributed equally to this work.

lactate (ML A) yield to more than 65 % by adding alkali metal salts during the hydrothermal synthesis of Sn-Beta with sucrose as feedstock. They attributed this improvement to the metal ions filling the framework defect thereby neutralizing the Brønsted acid produced by the silica hydroxyl group. Yang et al.[12] prepared Mg-Sn-Beta zeolites by co-impregnation method from parent dealuminated zeolites, achieving an 48 % ML A yield from glucose. Dong et al.[19] prepared Zn-Sn-Beta by solid-state ion exchange and achieved 54 % lactic acid yield from glucose. Both studies concluded that metal ions replaced the silanol protons, i.e. grafted to the framework, and an increase in Lewis acid or base sites was observed. A more comprehensive summary is listed in Supporting Information (Table S3.5). Although the combination of metal ions with Sn-Beta catalysts were reported in various studies to obtain higher yields of ML A or lactic acid, these studies only concern the relationship between the metal ions and the overall change in acidity and basicity.

In this work, we focus on the effect of the metal ions position on the local connectivity of the individual Sn sites mainly in the open or closed state, and the resulting catalytic activity. Originally, a synthetic scheme is proposed to create a nest of silica hydroxyl groups in the proximity of Sn as an additional anchor point to place Ni, Co, or other metal cations beside the Sn sites by ion exchange. As a result, Sn-Ni-Beta exhibit extremely high glucose isomerization activity and ML A yield. By comparison with different methods and using a series of characterization techniques such as solid-state magic-angle spinning nuclear magnetic resonance (MAS NMR), X-ray photoelectron spectroscopy (XPS), transmission electron microscopy (TEM), spectroscopic analysis, and probe-temperature-programmed desorption (TPD), we attribute this catalytic ability to the precisely control of the metal ion position resulting in a stable open state of the Sn sites. The stabilizing effect of the adjacent metal cations was confirmed by calculating the energy profile of the different open and closed Sn sites using density functional theory (DFT).

Results and Discussion

In the previous literature, the introduction of metal ions could be briefly classified as being introduced during the hydrothermal synthesis of Sn-Beta or for the simultaneous or sequential introduction of Sn in the DA-Beta obtained by dealumination. However, with all these methods relative positions of Sn and Ni atoms cannot be controlled.[20] In this study, a Sn-Al gel was used as metal source to synthesize Sn-Al-Beta to control adjacent metal sites, which then was selectively dealuminated to produce defects. The metal ions were subsequently inserted into the defects, thus ensure the spatial proximity of metal ions to Sn sites inherits from the Sn-Al gel and Sn-Al-Beta. For a typical Sn-Ni-Beta catalyst, tetraethylammonium fluoride was used as a template to synthesize a gel containing both Sn and Al, then co-precipitation at 140 °C for 10 days to obtain the Sn-Al-Beta. The molar ratio of a typical gel is SiO_2 : $0.008\,SnO_2$: $0.004\,Al_2O_3$: 0.54 TEAF : $11\,H_2O$. The final catalyst was obtained by gentle dealumination and ion exchange with 2 M nickel nitrate solution after calcination. For comparison, we also prepared Sn-Beta using widely reported hydrothermal synthesis and post-synthesis methods,[21,22] which were labeled as Sn-Beta-F and Sn-Beta-PS, respectively. Detailed synthesis schemes are recorded in the Supporting Information S.1. The proportions of Si, Sn and Ni in the catalysts were determined by Inductively Coupled Plasma Optical Emission Spectrometer (ICP-OES) and X-Ray Fluorescence (XRF) spectrometer (Table S2.1). The elemental mapping shows that the Sn and Ni ion dispersion in Sn-Ni-Beta is homogeneous and not affected by the ion exchange degree (Figure 1, S2.1). Clear lattices are observed in the HRTEM images, consistent with the typical diffraction peaks of the BEA* topology, in line with the X-ray diffraction (XRD) pattern (Figure S2.2). A similar pattern of Sn-Beta-PS suggests that the dealumination process, and thus the Al removal, does not significantly affect the BEA* zeolite structure. In agreement with literature,[22] an insignificant decrease of the relative crystallinity of the post-treated Sn-Beta-PS, (calculated according to the area of peaks at 2θ of 7.9° and 22.6°) indicates that Sn cannot completely replace all Al and that defects remain in the final zeolite. The absence of tin dioxide in the TEM images and the absence of its typical diffraction peaks prove that no significant bulk tin oxide was formed during the synthesis process for all catalysts. The porous structure of the catalysts were investigated by N_2 sorption isotherm (Table S2.2). The Sn-Beta-PS obtained from the post-treatment shows a larger mesoporous volume and outer surface area due to the dealumination treatment. For Sn-OH-Beta, which was also obtained by dealumination, an increase in micropore volume is observed compared to Sn-Al-Beta. This is different from

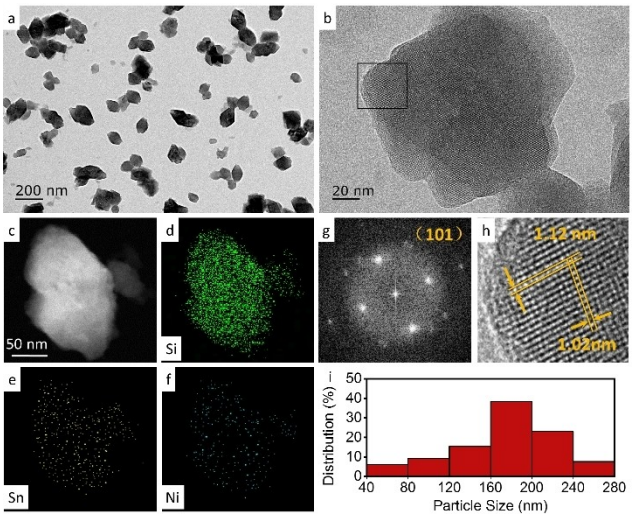

Figure 1. a) Low-resolution TEM images of Sn-Ni-Beta. b) High-resolution (HR) TEM images of Sn-Ni-Beta. c)–f) HAADF-STEM images and elemental maps of Sn-Ni-Beta, including d) Si, e) Sn, and f) Ni. g), h) The oriented lattice fringes of the corresponding boxed regions and the fast Fourier transform of the HRTEM. i) Particle size distribution obtained from low-resolution TEM image analysis.

Sn-Beta-PS, and this may be due to the lower Si-Al ratio of Sn-Al-Beta, which forms fewer vacancies after dealumination and cannot be connected to form mesopores, thus leading to an increase in micropore volume. After metal ion exchange, the micropore volume return to a level similar to that of Sn-Al-Beta. This may relate to the exchange of metal ions for the silanol protons. It is confirmed by the Fourier transmission infrared (FT-IR) spectroscopy, the multiple peaks centered on 3527 cm^{-1} and 1091 cm^{-1} are significantly attenuated after zeolite ion exchange, and a new absorption peak appears near 960 cm^{-1}, implying the presence of metal atoms attached to the zeolite framework (Figure S2.3).[23] Comparing the X-ray photoelectron spectroscopy (XPS) results (Figure 4b) of Sn elements in various catalysts, the binding energies in Sn-Ni-Beta, Sn-Beta-F, and Sn-Beta-PS with respect to Sn $3d_{5/2}$ show a symmetrical signal centered at approximately 487.8 eV without a sub-peak centered at 486.6 eV, which is related to Sn $3d_{5/2}$ of SnO_2.[12,24] It can be confirmed that Sn atoms are highly dispersed in zeolites, and no SnO_2 crystal phase is formed. Moreover, the result is also confirmed by ultraviolet-visible diffuse reflection spectroscopy (UV/Vis DRS; Figure S2.4), in which a significant absorption peak only appears near 200 nm.

The catalytic reaction of glucose to MLA in methanol/water, of which the reaction network is presented in Scheme 1, was carried out in a stainless steel reactor at 180 °C. Figure 2 collects the reaction data for the various catalysts. It shows that the highest MLA yield was achieved over the Sn-Ni-Beta catalyst, reaching 71.2 % yield of MLA within 3 h, and 10.3 % yield of methyl vinyl glycolate (MVG) as the main side-product. For comparison, we examined catalysts only containing either Sn or Ni. Among them, Sn-OH-Beta was used, which obtained from the same synthesis process as Sn-Ni-Beta, except that the Ni^{2+} ion exchange was omitted. The synthesis method of Ni-Beta is provided in the Supporting Information S.1. Sn-Beta-F and Sn-Beta-PS were synthesized according to references.[21] The results show the highest MLA yield (47.4 %) for the Sn-only catalysts, which is achieved over Sn-Beta-F, while the highest MVG yield (17.9 %) is reached over Sn-Beta-PS. It is well known that both MLA and MVG are derived from the C3 and C4 (C2) products produced by the retro-aldol condensation of fructose and glucose, respectively, and subsequently obtained by similar chemical transformations (e.g., dehydration, keto-enol tautomerization, 1,2-hydride shift, and internal Cannizzaro reaction).[25] Early work has shown that the formation of MVG from C4 sugars can be stimulated by catalytic sites in confined space and operating at higher temperature.[26] The selectivity difference between these two products in this work, starting from glucose, may arise from the different glucose isomerization abilities of the catalysts. Indeed, we examined the kinetic performance of several zeolites catalyzing the conversion of glucose to fructose. When normalizing the initial isomerization rate to the catalyst mass, Sn-Ni-Beta exhibits the highest rate of fructose formation (Table 1). When Ni is present in the zeolite without Sn, glucose is hardly converted to MLA or fructose. In addition, Sn-Ni-Beta can also catalyze the conversion of mono- and disaccharides other than glucose to MLA with appreciable yields (Table S3.1). Under the same

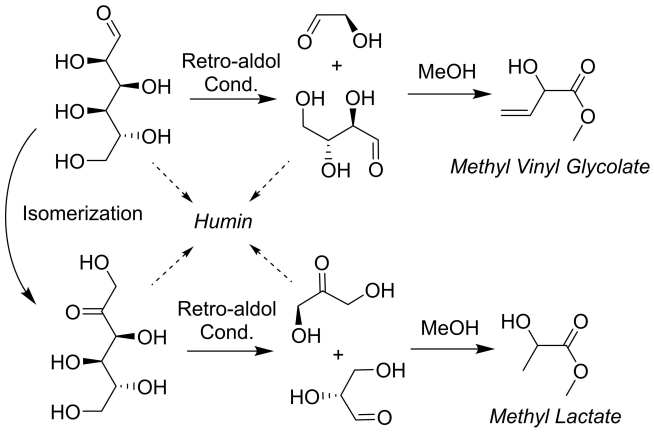

Scheme 1. Reaction pathway from glucose to MLA, MVG and side reactions.

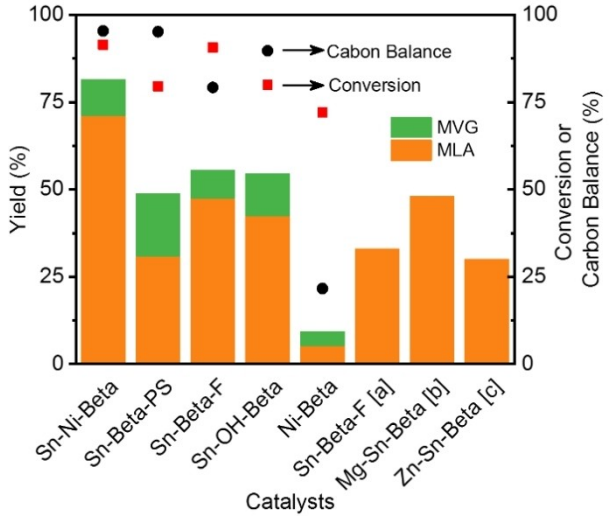

Figure 2. Glucose conversion to methyl lactate or fructose with different catalysts. Reaction conditions for catalyzing glucose to methyl lactate: glucose (500 mg), catalyst (200 mg), mixed solvent (30 ml, MeOH/H_2O, w/w = 9) were stirred in an autoclave at 180 °C and 600 rpm for 3 hours. Reaction conditions for Sn-Beta-F [a],[9] Mg-Sn-Beta [b],[12] and Zn-Sn-Beta [c][19] are those given in the respective references.

Table 1: First order glucose isomerization rate constants for catalysts at 373 K. The relative error of the data was estimated to be 10%. Estimates of data errors are recorded in Supporting Information Note S4.1.

Catalysts	Isomerization rate constants [10^{-5} mol fru.· (mol open Sn)$^{-1}$· (mol glu. M^{-3})$^{-1}$·s^{-1}]	[10^{-8} mol fru.· (g catalyst)$^{-1}$· (mol glu. M^{-3})$^{-1}$·s^{-1}]
Sn-Ni-Beta	76.30	51.11
Sn-Beta-F	66.58	21.30
Sn-Beta-PS	7.99	3.98
Sn-OH-Beta	62.00	30.77

reaction conditions with fructose or sucrose as substrate, the yields of MLA are 74.8 % and 68.5 %, respectively.

To better elucidate the role of Ni, we prepared Sn-Ni-Beta with different Ni contents (Table S3.2). Interestingly, it is found that there is a positive correlation between the MLA yield and the Ni content. Therefore, the presence of Ni governs the competitive selectivity towards MLA. Subsequently, we performed Ni^{2+} ion exchange on Sn-Beta-F and Sn-Beta-PS. A significant increase in the yield of MLA (57.5 %) is also found after the introduction of Ni into Sn-Beta-PS (Ni-Sn-Beta-PS), albeit lower compared with the results with Sn-Ni-Beta (Table S3.3). It is worth noting that the Ni content of Ni-Sn-Beta-PS is higher than that of Sn-Ni-Beta (Table S2.1) and therefore contains sufficient Ni to cause a selectivity shift towards MLA. Overall, this catalytic study shows that a small number of nickel atoms present in specific positions in Sn-Beta zeolites can cause a dramatic change in the selectivity of glucose conversion.

The lifetime of the Sn-Ni-Beta catalyst was examined and the metal content of each catalyst sample was determined by ICP-OES after each cycle. The loss of nickel is significant and the yield of MLA shown in the third cycle is very close to that of Sn-Beta-F (Table S3.4, Figure S3.1). Accordingly, we propose a regeneration method besides calcination, i.e. a re-ion exchange of Sn-Ni-Beta prior to calcination regeneration. It is worth pointing out that the nickel nitrate solution used is the same solution that was involved in the first batch of Sn-Ni-Beta synthesis, thus causing no additional waste of metal salts or environmental stress. After the reintroduction of Ni, the yield of MLA and MVG returns to a level comparable to that of the fresh catalysts (Figure S3.1). This suggests that despite the loss of Ni species, the nests of silica hydroxyl groups that provide the specific sites in which Ni is located are retained and the considerable recovery of catalytic capacity can be achieved by re-ion exchange.

Sn sites, as the Lewis acid center, activate the carbonyl group for glucose conversion and initiate isomerization and other reactions. The role of Ni is unclear. However, the activation enthalpy and activation entropy exhibited by Sn-Ni-Beta in the glucose isomerization reaction are very similar to those of Sn-Beta-F, (Table S4.1) indicating that the introduction of Ni does not directly lead to a significant change in the reaction pathway. This is also indicated by the fact that Ni-Beta does not exhibit any catalytic activity. What can be inferred is the change of Sn state by adding Ni. With the help of basic probe molecules, we tried to identify the impact of the presence of Ni on the properties of the Sn sites. After the adsorption of deuterated acetonitrile on the catalyst, two types of Sn sites, open and closed, could be distinguished and quantified by FT-IR spectroscopy.[27] Figure 3a shows the FT-IR spectra of three catalysts after adsorption of CD_3CN. Based on the quantitative study at 303 K, Sn-Ni-Beta contains the highest proportion of open Sn sites with a ratio of 2.37 to the number of closed sites (Inset in Figure 3a, Table S5.1). ^{119}Sn MAS NMR, another technique that can distinguish different Sn sites such as the open and closed forms,[6,15,28] confirms this result (Figure 3b). For several catalysts after drying at 393 K under vacuum,

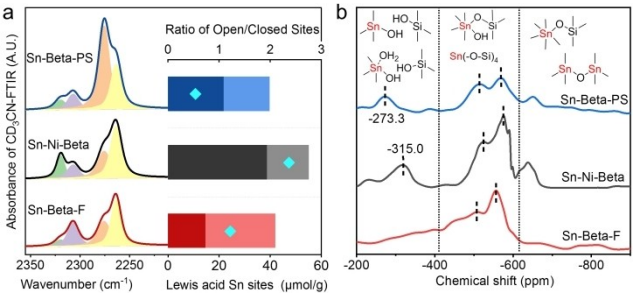

Figure 3. a) The transmission infrared spectrum of Sn-Beta-PS, Sn-Ni-Beta, Sn-Beta-F adsorbed CD_3CN in vacuum at 30 °C, and quantification of the two types of Sn sites of the catalysts. Dark color represents open sites; light color represents closed sites. The detailed quantitative data is recorded in the Supporting Information. b) ^{119}Sn solid state NMR spectrum of Sn-Ni-Beta, compared with Sn-Beta-F and Sn-Beta-PS.

chemical shifts below −635 ppm are assigned to the hydrated closed Sn sites. The continuous signals, between −410 ppm and −635 ppm, can be assigned to the convolution of octahedral hydrated open Sn sites, and dehydrated closed Sn sites. The signals above −400 ppm are assigned as partially or fully dehydrated penta-coordinated or tetrahedral open Sn sites.

Next to the identification of the Sn sites, it is also found that Sn-Ni-Beta shows the highest atomic utilization of Sn, i.e., the highest proportion of Sn atoms exhibiting Lewis acidity, accounting for 92.6 % of the total Sn atoms (Table S5.1), while this value is only 73.3 % and 70.3 % for Sn-Beta-F and Sn-Beta-PS, respectively. Similar results are further demonstrated by pyridine-FTIR, which is recorded in the Supporting Information S.6. Although the method cannot distinguish between open or closed Sn sites, the possible contribution of Brønsted acid in the catalysts is ruled out by this result. No recognizable absorption peak is observed near 1540 cm^{-1}. Ammonia-TPD was carried out on the catalysts and the NH_3 desorption below and above 300 °C were recorded (Figure S7.1, Table S7.1). In order to exclude the effect of bound water in the catalyst, the signal during temperature rise of samples without adsorbed NH_3 was used as a baseline. The result shows that Sn-Ni-Beta contains the highest number of total acidic sites and exhibits the highest desorption peak at 300–500 °C. This indicates that the introduction of Ni renders more acidic sites than the Sn-only catalyst and contributes mainly to the increase in strong acidic sites, which is consistent with the results of quantification using CD_3CN and pyridine. This means that benefiting from the specific locations of the Ni in the Sn-Beta structure, more open Sn sites are formed, as well as higher Lewis acid strength.

It is necessary to investigate which key position or state of Ni in the Sn-Beta structure leads to the activity improvement of Sn as the Lewis acid center. First of all, the presence of large nickel oxide in the zeolite can be ruled out with the help of UV/Vis DRS and XRD diffraction analysis (Figure S2.4, S2.2). XPS analysis can inform about the electron density of the Ni element. It shows that Ni in Sn-Ni-Beta has a higher photoelectron binding energy of $2p_{3/2}$ and $2p_{1/2}$ than

that of Ni-Sn-Beta-PS (Figure 4a). This can be attributed to the higher oxidation state and lower electron density of Ni formed in Sn-Ni-Beta. The proximity of atoms impacts the electronic state of the Sn site. Dijkmans et al.[10] pointed out that the open Sn site is stabilized by a coordinated water molecule. Corma et al.[29] found that when Sn connected to the oxygen atom from guest molecule, the electron density will be pushed from the center of Sn into the lobes of the s*(Sn–O) orbitals located on the oxygen atoms, which is the characteristic of electron pumping. Interestingly, we also find a weak electron counteraction of Ni for Sn from the X-ray photoelectron spectrum of the Sn element (Figure 4b). Considering that electron cloud effects are only possible on the microscale, it can be inferred that Ni should be in the vicinity of Sn–O, as such being able to influence the bridging oxygen of the neighboring Sn. Suggestions of the location of Ni in the Sn zeolite are presented in Figures 4c–e. Ni can be present in the zeolite in two ways: as a divalent cation charge balanced with the zeolite structure; and as a semi-framework form co-existing with silica hydroxyl (Figure 4c). When Sn is present alone, it can be broadly classified into open and closed states (Figure 4d), and for clarity, the case of hydration is not considered at this stage. When Ni and Sn are present in adjacent positions (Figure 4e), the increase in the binding energy of Ni $2d_{1/2}$ indicates an increase in the number of framework and semi-framework species. More Ni–O bonds than Si–O are involved in the framework associated with the first coordination sphere of Sn, which allows for the stable presence of more open Sn sites. As mentioned in the synthetic scheme, the relative positions of the Sn and Ni ions are inherited from several parent zeolites, including Sn-Al-Beta and its mildly dealuminated Sn-OH-Beta (Figure 5b). This proximate structural inheritance is demonstrated by their characterization. As can be seen from the ^{27}Al MAS NMR spectra of the Al-related samples (Figure 5a), the chemical shift of the tetrahedrally coordinated Al corresponding to Sn-Al-Beta is about 50 ppm, unlike the chemical shifts of Al near 53 ppm and 0 ppm observed on commercial Al-Beta. This signal is also observed in the Sn-Al hydroxide gel, which is the metal source used for the synthesis of zeolites. It can be assumed that the interaction of Sn and Al with hydroxyl groups leads to the appearance of a signal, and the adjacent structural configurations of Sn and Al are inherited into the zeolites framework when the Sn-Al hydroxide gel was used as a raw material for the synthesis of zeolites.

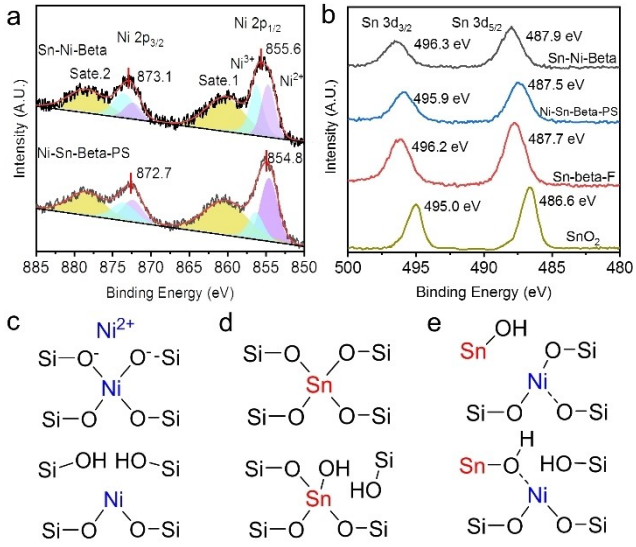

Figure 4. a) X-ray photoelectron spectra (XPS) binding energy of Ni $2p_{1/2}$ and $2p_{3/2}$ for Sn-Ni-Beta and Ni-Sn-Beta-PS. b) XPS binding energy of Sn $3d_{3/2}$ and $3d_{5/2}$ for Sn-Ni-Beta, Ni-Sn-Beta-PS, Sn-Beta-F, and SnO_2. c) Possible states of Ni present alone in zeolites. d) Possible states of Sn present alone in zeolites. e) Possible states of Ni adjacent to Sn in zeolites.

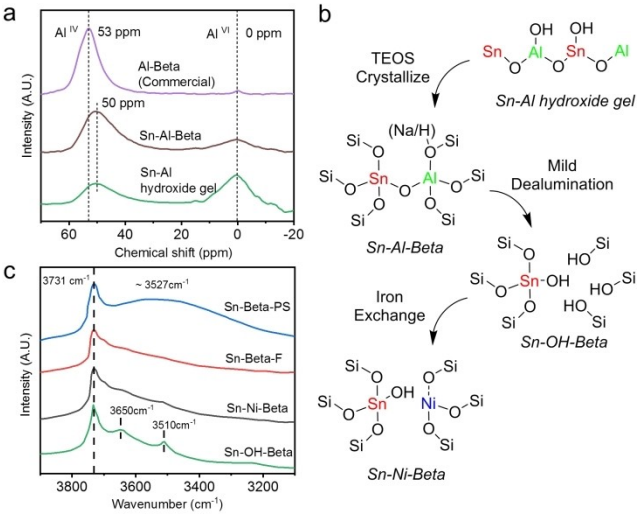

Figure 5. a) ^{27}Al MAS NMR spectra of zeolites and Sn-Al hydroxide gel. b) Synthesis process of Sn-Ni-Beta and succession of adjacent structures in zeolite synthesis steps. c) Diffuse reflectance infrared Fourier transform spectra in the hydroxyl stretching vibration region of catalysts.

This is further supported by the analysis from EXAFS, which was started on an energy-optimized Sn-Ni-Beta model obtained by DFT calculations (see next section). The results show that in addition to three at 1.96 Å and one at 2.05 Å framework oxygen, one Ni at 3.22 Å, as well as one Si at 3.24 Å and one Si at 3.28 Å are resolved (Table S9.1). For a clearer distinction, the EXAFS were represented in two dimensions with the help of wavelet transform analysis (WTA), and the signals were localized in both k and R space (Figure S9.3). A clear separation of the two lobes in the range $R = 2.2$–3.0 Å and $k = 7.1$–10 Å, attributed to the contributions from the Sn-Si and Sn-Ni paths, respectively, can be observed from the full-range EXAFS WT 2D plots.

The silica hydroxyl group as the terminal of zeolite skeleton is the main site for connecting other metal atoms, so we investigated the hydroxyl groups of Sn-Ni-Beta and its parent, Sn-OH-Beta. We used diffuse reflectance infrared Fourier transform (DRIFT) spectroscopy rather than conventional transmission FT-IR because of the former's higher sensitivity and signal-to-noise ratio for OH groups.[30] As seen in the spectrum, Sn-Beta-PS exhibits a broad hydroxyl absorption peak centered around 3527 cm^{-1}, which can be attributed to the multi-environmental hydroxyl groups in

zeolites (Figure 5c). However, this broad peak is not observed in Sn-Ni-Beta and Sn-Beta-F, which indicates that the pores of Sn-Ni-Beta are hydrophobic because fluoride was used as a mineralizer in synthetic gels.[31] This result is also confirmed by the adsorption isotherm analysis of water and methanol for several samples (Supporting Information Note S8.1). It is noteworthy that two distinct absorption peaks are found at 3510 cm^{-1} and 3650 cm^{-1} before the final step of Sn-Ni-Beta ion exchange, i.e. Sn-OH-Beta, and disappear with Ni^{2+} ion exchange. It is much narrower than the broad peak at 3527 cm^{-1}. This means that the hydroxyl groups attributed to these peaks are in the more uniform environment. These two peaks differ from the absorption peaks attributed to the Brønsted acid site exhibited by commercial H-Beta and Sn-Al-Beta (Figure S2.5).

Based on the previous structural exploration, this can be attributed to the silica hydroxyl nests specifically associated with the Sn site, providing an anchor point for ion-exchanged Ni that can affect the stability of openness for Sn. In addition, the absorption peaks at 3510 cm^{-1} as well as 3650 cm^{-1} do not appear in Sn-Beta-F, pointing out that the adjacent Sn-Ni structure cannot be obtained by ion exchange of Sn-Beta-F either. In fact, due to the very small number of silica hydroxyl groups in the pore, it is almost impossible to dope Ni into Sn-Beta-F under the same ion-exchange conditions (Table S2.1).

By the exchange of other metal ions for Sn-OH-Beta, we demonstrate that Ni is not the only metal that can stabilize the open state of Sn. The nitrate solutions of Co^{2+}, Mn^{2+}, Mg^{2+}, and other metal ions were used to replace nickel nitrate for ion exchange in catalyst synthesis. When these prepared catalysts were applied for the conversion of glucose, the MLA yield is also improved, e.g., being 68.4 % for the Co ion-exchanged catalyst under the same conditions. A similar characterization can explain this improvement: the XPS results of Co $2p_{3/2}$ and $2p_{1/2}$ show a shift of the binding energy to a lower position. The binding energy at $2p_{3/2}$ of Mn shifts very slightly. The $2p_{1/2}$ binding energy shift of Mg is almost imperceptible, and correspondingly, the catalytic ability for glucose is also weakly improved (Table S3.3). Similarly, Sn-Co-Beta was tested for ammonia-TPD, and the result shows that it has a stronger Lewis acidity than Sn-Beta-F, Sn-Beta-PS, and Sn-OH-Beta (Figure S7.2). Therefore, identifying the common characteristics of metal ions that can stabilize open Sn sites is one of the directions for the following work.

DFT calculations were further performed to understand the structural properties of closed and open Sn sites in several Sn-Beta as well as the effect of Ni modification. The dealumination of Sn-Al-Beta leads to the formation of defected Sn-OH-Beta with a silica hydroxyl nest (Figure 6). Such an Sn-OH-Beta model was constructed from the original Sn-Si-Beta model by removing one neighboring Si around the Sn sites (Figure S10.1). Under dry conditions, an Sn-defect-Beta (closed) can be formed from Sn-OH-Beta by removing two H_2O molecules, in which two silica hydroxyls (Si– OH) form a Si– O– Si structure and another Si– OH reacts with Sn– OH forming a Si– O– Sn structure. In this closed state, the DFT-predicted bond length of Sn– O is

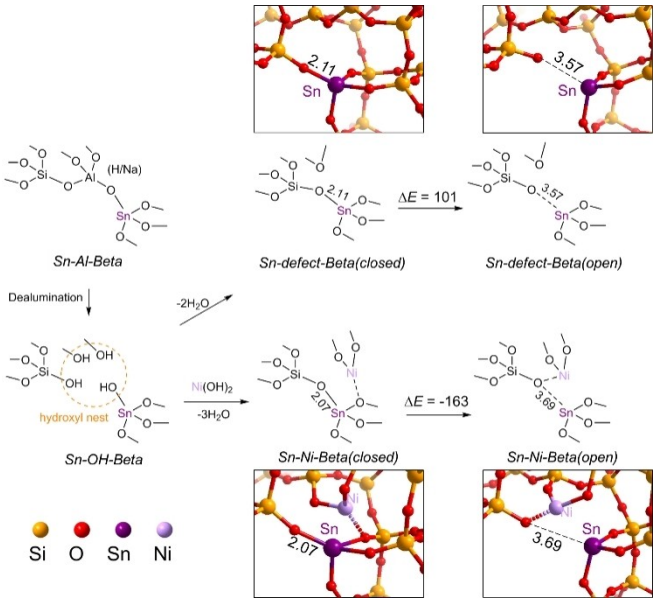

Figure 6. Effect of Ni on the stabilization of open Sn site in Beta zeolite. The structures of open and closed Sn sites were proposed based on DFT calculations. Energy changes (ΔE) and atomic distances are given in kJ mol^{-1} and angstrom [Å], respectively.

2.11 Å. The bond breaking of Sn–O in Sn-defect-Beta (closed) can form a metastable state of Sn-defect-Beta (open) with the bond length of Sn–O elongated to 3.57 Å, in which the Sn site shows a three-fold close SiO^- coordination and another one coordination by a distant charge-balancing SiO^-. Such a DFT model is consistent with the inner/outer sphere Sn site model proposed by the previous work based on EXAFS analysis.[10] The formation of sterically separated $(SiO)_3Sn^+$ and SiO^- ion-pair was assumed to be a result of the restriction of their lattice positions, and such named frustrated Lewis pairs may behave as both acid and base to activate reagents with high catalytic reactivity. However, in the case of the Sn-defect-Beta model in this study, it is found that the formation of such an open state is energetically unfavorable by 101 kJ mol^{-1}, and the energy compensation is related to the formation of the Sn–O bond from the terminal SiO^- and coordinately unsaturated Sn site induced by the flexibility of zeolite framework. In contrast, the introduction of Ni is found to stabilize the terminal SiO^-, which maintains the separation of the unsaturated Sn site as an open state. The energy change for Sn-Ni-Beta from the closed to open Sn site is strongly favorable by -163 kJ mol^{-1}, which suggests that the presence of Ni is able to promote the formation of more open Sn sites in Sn-OH-Beta zeolites. This is consistent with the above FT-IR results using acetonitrile probes operated under almost dry conditions. The results from EXAFS further demonstrate the existence of the structure of Sn-Ni-Beta provided in Figure 6.

Next, we considered the transformations of closed to open Sn sites with the presence of water (Figure S10.2). The traditional hydrothermally synthesized Sn-Beta was represented by a defect-free Sn-Si-Beta. The hydrolysis of one Sn–O bond in Sn-Si-Beta can form either Sn^{IV}–OH site in

an open state [Sn^{IV}(OH)-Si(OH)-Beta] or Sn^{V}–OH in a penta-coordination [Sn^{V}(OH)–Si(OH)-Beta]. These processes require activation barriers of 90–98 kJ mol^{-1} with endothermicities by 70–92 kJ mol^{-1}. In contrast, the formation of open Sn sites in Sn-defect-Beta and Sn-Ni-Beta by water assistance is strongly exothermic by −208–−125 kJ mol^{-1} with neglectable activation barriers. This suggests the Sn sites in Sn-defect-Beta and Sn-Ni-Beta are more likely stabilized as open states under the involved aqueous conditions, in agreement with our ^{119}Sn MAS NMR results.

Conclusion

In this work, a synthetic scheme of Sn-Ni-Beta is proposed, in which a small amount of Ni is introduced into the Sn-adjacent correlation site in the Sn-Beta zeolite via ion exchange, effectively constructing a more stable open Sn site for the catalyst. The large number of stable open Sn sites allowed the catalyst to exhibit a higher apparent catalytic activity for the isomerization of glucose as well as its conversion to MLA and MVG. The proposed synthetic scheme can be adapted to other metal ions in the final step, in which they are conveniently inserted into the nests of silica hydroxyl groups constructed by neighboring Sn sites. This considerably extends the versatility of this synthetic approach: in the present work, in addition to Ni^{2+}, Co^{2+} and Mn^{2+} also present a role in stabilizing open Sn sites, and a wider range of catalytic potentials of adjacent bimetal zeolites can be developed in future work.

Acknowledgements

The authors acknowledge the financial support from the National Natural Science Foundation of China projects (nos.52276220), National Key R&D Program of China (2018YFB1501504), Key Technologies R&D Program of Guangdong Province (2020B1111570001).

Conflict of Interest

The authors declare no conflict of interest.

Data Availability Statement

The data that support the findings of this study are available in the Supporting Information of this article.

Keywords: Carbohydrate Conversion · Heterogeneous Catalysis · Lewis Acid · Methyl Lactate · Sn-Beta Zeolite

[1] S. De, A. S. Burange, R. Luque, *Green Chem.* **2022**, *24*, 2267.
[2] E. Peeters, G. Pomalaza, I. Khalil, A. Detaille, D. P. Debecker, A. P. Douvalis, M. Dusselier, B. F. Sels, *ACS Catal.* **2021**, *11*, 5984.
[3] S. Van de Vyver, C. Odermatt, K. Romero, T. Prasomsri, Y. Román-Leshkov, *ACS Catal.* **2015**, *5*, 972.
[4] J. D. Lewis, S. Van de Vyver, Y. Román-Leshkov, *Angew. Chem. Int. Ed.* **2015**, *54*, 9835; *Angew. Chem.* **2015**, *127*, 9973.
[5] a) R. Bermejo-Deval, R. Gounder, M. E. Davis, *ACS Catal.* **2012**, *2*, 2705; b) Y. Román-Leshkov, M. Moliner, J. A. Labinger, M. E. Davis, *Angew. Chem. Int. Ed.* **2010**, *49*, 8954; *Angew. Chem.* **2010**, *122*, 9138.
[6] R. Bermejo-Deval, M. Orazov, R. Gounder, S.-J. Hwang, M. E. Davis, *ACS Catal.* **2014**, *4*, 2288.
[7] a) T. R. Josephson, R. F. DeJaco, S. Pahari, L. Ren, Q. Guo, M. Tsapatsis, J. I. Siepmann, D. G. Vlachos, S. Caratzoulas, *ACS Catal.* **2018**, *8*, 9056; b) P. Wolf, M. Valla, F. Núñez-Zarur, A. Comas-Vives, A. J. Rossini, C. Firth, H. Kallas, A. Lesage, L. Emsley, C. Copéret, et al., *ACS Catal.* **2016**, *6*, 4047.
[8] E. Peeters, S. Calderon-Ardila, I. Hermans, M. Dusselier, B. F. Sels, *ACS Catal.* **2022**, *12*, 9559.
[9] X. Yang, Y. Liu, X. Li, J. Ren, L. Zhou, T. Lu, Y. Su, *ACS Sustainable Chem. Eng.* **2018**, *6*, 8256.
[10] J. Dijkmans, M. Dusselier, W. Janssens, M. Trekels, A. Vantomme, E. Breynaert, C. Kirschhock, B. F. Sels, *ACS Catal.* **2016**, *6*, 31.
[11] J. Iglesias, J. Moreno, G. Morales, J. A. Melero, P. Juárez, M. López-Granados, R. Mariscal, I. Martínez-Salazar, *Green Chem.* **2019**, *21*, 5876.
[12] X. Yang, B. Lv, T. Lu, Y. Su, L. Zhou, *Catal. Sci. Technol.* **2020**, *10*, 700.
[13] S. Tolborg, I. Sádaba, C. M. Osmundsen, P. Fristrup, M. S. Holm, E. Taarning, *ChemSusChem* **2015**, *8*, 613.
[14] a) B. C. Bukowski, J. S. Bates, R. Gounder, J. Greeley, *Angew. Chem. Int. Ed.* **2019**, *58*, 16422; *Angew. Chem.* **2019**, *131*, 16574; b) J. R. Di Iorio, B. A. Johnson, Y. Román-Leshkov, *J. Am. Chem. Soc.* **2020**, *142*, 19379; c) M. J. Cordon, J. W. Harris, J. C. Vega-Vila, J. S. Bates, S. Kaur, M. Gupta, M. E. Witzke, E. C. Wegener, J. T. Miller, D. W. Flaherty, et al., *J. Am. Chem. Soc.* **2018**, *140*, 14244.
[15] A. V. Yakimov, Y. G. Kolyagin, S. Tolborg, P. N. R. Vennestrøm, I. I. Ivanova, *J. Phys. Chem. C* **2016**, *120*, 28083.
[16] T. R. Josephson, G. R. Jenness, D. G. Vlachos, S. Caratzoulas, *Microporous Mesoporous Mater.* **2017**, *245*, 45.
[17] J. S. Bates, B. C. Bukowski, J. W. Harris, J. Greeley, R. Gounder, *ACS Catal.* **2019**, *9*, 6146.
[18] a) C. Flores, N. Batalha, N. R. Marcilio, V. V. Ordomsky, A. Y. Khodakov, *ChemCatChem* **2019**, *11*, 568; b) C. J. Heard, L. Grajciar, F. Uhlík, M. Shamzhy, M. Opanasenko, J. Čejka, P. Nachtigall, *Adv. Mater.* **2020**, *32*, 2003264.
[19] W. Dong, Z. Shen, B. Peng, M. Gu, X. Zhou, B. Xiang, Y. Zhang, *Sci. Rep.* **2016**, *6*, 26713.
[20] a) J. R. Di Iorio, C. T. Nimlos, R. Gounder, *ACS Catal.* **2017**, *7*, 6663; b) M. Yabushita, R. Osuga, A. Muramatsu, *CrystEngComm* **2021**, *23*, 6226.
[21] H. J. Cho, N. S. Gould, V. Vattipalli, S. Sabnis, W. Chaikittisilp, T. Okubo, B. Xu, W. Fan, *Microporous Mesoporous Mater.* **2019**, *278*, 387.
[22] J. Zhang, L. Wang, G. X. Wang, F. Chen, J. Zhu, C. T. Wang, C. Q. Bian, S. X. Pan, F. S. Xiao, *ACS Sustainable Chem. Eng.* **2017**, *5*, 3123.
[23] a) K. Chalupka, R. Sadek, L. Valentin, Y. Millot, C. Calers, M. Nowosielska, J. Rynkowski, S. Dzwigaj, H. Kazemian, *J. Chem.* **2018**, *2018*, 7071524; b) I. Kiricsi, C. Flego, G. Pazzuconi, W. O. Parker, Jr., R. Millini, C. Perego, G. Bellussi, *J. Phys. Chem.* **1994**, *98*, 4627; c) S. R. Tomlinson, T. McGown, J. R. Schlup, J. L. Anthony, A. Wada, *Int. J. Spectrosc.* **2013**, *2013*, 961404.

[24] W. Dai, Q. Lei, G. Wu, N. Guan, M. Hunger, L. Li, *ACS Catal.* **2020**, *10*, 14135.
[25] Z. Huang, L. J. Liu, J. F. Zhang, H. M. Yang, S. Fu, T. H. Liu, H. Q. Yang, C. W. Hu, *J. Phys. Chem. C* **2020**, *124*, 13102.
[26] R. de Clercq, M. Dusselier, C. Christiaens, J. Dijkmans, R. I. Iacobescu, Y. Pontikes, B. F. Sels, *ACS Catal.* **2015**, *5*, 5803.
[27] J. W. Harris, M. J. Cordon, J. R. Di Iorio, J. C. Vega-Vila, F. H. Ribeiro, R. Gounder, *J. Catal.* **2016**, *335*, 141.
[28] a) L. Botti, D. Padovan, R. Navar, S. Tolborg, J. S. Martinez-Espin, C. Hammond, *ACS Catal.* **2020**, *10*, 11545; b) G. Qi, Q. Wang, J. Xu, Q. Wu, C. Wang, X. Zhao, X. Meng, F. Xiao, F. Deng, *Commun. Chem.* **2018**, *1*, 22.
[29] M. Boronat, A. Corma, M. Renz, P. M. Viruela, *Chem. Eur. J.* **2006**, *12*, 7067.
[30] I. Halasz, B. Moden, A. Petushkov, J.-J. Liang, M. Agarwal, *J. Phys. Chem. C* **2015**, *119*, 24046.
[31] D. T. Bregante, D. S. Potts, O. Kwon, E. Z. Ayla, J. Z. Tan, D. W. Flaherty, *Chem. Mater.* **2020**, *32*, 7425.

Zeolite Catalysis

P. Sun, C. Liu, H. Wang, Y. Liao, X. Li,
Q. Liu, B. F. Sels, C. Wang* – **e202215737**

Rational Positioning of Metal Ions to Stabilize Open Tin Sites in Beta Zeolite for Catalytic Conversion of Sugars

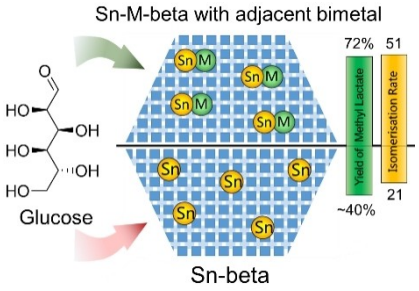

Metal ions such as Ni^{2+}, Co^{2+}, and Mn^{2+} were positioned within Sn-Beta zeolite to form adjacent bimetallic catalytically active sites with stable open Sn sites. The Sn-Ni-Beta catalyst selectively converts glucose to methyl lactate and methyl vinyl glycolate in methanol in high yields of 71.2% and 10.2%, respectively.